The G1/S transition is promoted by Rb degradation via the E3 ligase UBR5

Shuyuan Zhang[1], Lucas Fuentes Valenzuela[1], Evgeny Zatulovskiy[1], and Jan M. Skotheim[1,2,*]

[1]Department of Biology, Stanford University, Stanford, CA 94305
[2]Chan Zuckerberg Biohub, San Francisco, CA 94158
[*]Address correspondence to skotheim@stanford.edu

Abstract

Mammalian cells make the decision to divide at the G1/S transition in response to diverse signals impinging on the retinoblastoma protein Rb, a cell cycle inhibitor and tumor suppressor. Rb is inhibited by two parallel pathways. In the canonical pathway, cyclin D-Cdk4/6 kinase complexes phosphorylate and inactivate Rb. In the second, recently discovered pathway, Rb's concentration decreases during G1 through an unknown mechanism. Here, we found that regulated protein degradation via the E3 ubiquitin ligase UBR5 is responsible for Rb's concentration drop in G1. *UBR5* knockout cells have increased Rb concentration in early G1, exhibited a lower G1/S transition rate, and are more sensitive to inhibition of Cdk4/6. This last observation suggests that UBR5 inhibition can strengthen the efficacy of Cdk4/6 inhibitor-based cancer therapies.

One-Sentence Summary: The E3 ligase UBR5 progressively reduces the concentration of the retinoblastoma protein Rb during G1 to drive proliferation.

Main Text

The decision to divide often takes place in the G1 phase of the cell cycle and occurs in response to diverse input signals. Once taken, the decision to initiate DNA replication and divide is difficult to reverse despite changes to the input signals (*1*, *2*). From a molecular point of view, the commitment point at the G1/S transition in response to growth signals corresponds to the hyper-phosphorylation and inactivation of the transcriptional inhibitor Rb, the retinoblastoma protein (*1*, *3*, *4*). Hyper-phosphorylation of Rb frees the activating E2F transcription factors to drive expression of the cyclins E and A, which mostly form complexes with the cyclin-dependent kinase Cdk2. Active cyclin E/A-Cdk2 complexes then maintain Rb hyper-phosphorylation so that E2F-dependent transcription remains active (*5*). While the molecular basis of the commitment point to cell division is increasingly well understood, we know much less about how the upstream growth and differentiation input signals transmit quantitative information to the decision point.

Activating signals promoting the G1/S transition operate through at least two parallel pathways. First, growth factors initiate signals that increase the expression of cyclin D (*6*), which primarily forms a complex with the cyclin-dependent kinases Cdk4 and Cdk6 (*7*). Cyclin D-Cdk4/6 complexes then initiate the phosphorylation of Rb, possibly through hypo- or mono-phosphorylation (*8*, *9*), to promote the G1/S transition. A second parallel activating signal operates through the concentration of Rb itself, which we recently found to decrease as cells grow through G1 (*10*, *11*). Thus, the current model is that these two mechanisms cooperate to activate E2F-dependent transcription and initiate the cell cycle. Namely, cyclin D-dependent Rb hypo-phosphorylation shifts the dissociation constant (K_d) of Rb with E2F so that the decreasing Rb concentration can drop below K_d to release active E2F. Following the G1/S transition, Rb's concentration increases during S/G2/M to reset for the next cell cycle. Although several molecular mechanisms underlying cyclin D synthesis and Rb phosphorylation by cyclin D-Cdk4/6 have been elucidated (*8*, *12*), the molecular mechanism underlying the decrease in Rb concentration through G1 is unknown.

Here, we sought to determine the molecular mechanisms underlying Rb's concentration decrease through G1 (Fig. 1A), an important signal triggering the G1/S transition. We found that Rb is targeted for degradation in G1 by the E3 ligase UBR5. At the G1/S transition, Rb is stabilized by hyper-phosphorylation so that its concentration recovers for the next G1 phase. Disruption of this G1 Rb degradation mechanism decreases the G1/S transition rate and sensitizes cells to chemical inhibition of the parallel pathway based on Cdk4/6 activity.

Rb concentration dynamics are regulated by degradation

During early- to mid-G1 phase, the concentration of Rb protein continuously decreases to promote cell cycle entry (*10*)(Fig. 1B, Fig. S1A). Then, in late G1, the Rb concentration begins its recovery back to the initial concentration. This transition point in mid/late-G1 is marked by an increase in Cdk activity as assessed by the nuclear translocation of an HDHB-based sensor (*1*, *13*). These dynamics are relatively unique, as the concentrations of other G1/S pathway components remain constant throughout G1 phase (*10*, *11*). Moreover, a proteomics analysis revealed that Rb concentration changes far exceed those of a typical protein through the cell cycle (*14*). The dilution of Rb in G1 is an important input to the decision to divide as the Rb concentration is anti-correlated with the G1/S transition rate (*10*), and increasing the overall Rb concentration sensitizes cells to treatment by Cdk4/6 inhibitors (Fig. 1C, Fig. S1B).

To identify the mechanism regulating Rb concentration dynamics through the cell cycle, we examined both the synthesis and degradation of Rb protein in different cell cycle phases. We measured the mRNA concentration of *RB1* in different cell cycle phases by using flow cytometry to sort HMEC (telomerase-immortalized human mammary epithelial) cells expressing FUCCI (*15*) cell cycle reporters into G1 and S/G2 populations. We then performed qPCR or mRNA-Seq to measure *RB1* mRNA expression. The results showed that the *RB1* mRNA concentration did not significantly increase in S/G2 phase (Fig. 1D, Fig. S1C). We found a similar result when calculating *RB1* mRNA concentrations in different cell cycle phases using a published MERFISH dataset (*16*) (Fig. S1D). This indicates that Rb concentration dynamics are controlled by post-transcriptional mechanisms. To further investigate the synthesis dynamics of Rb protein, we measured the translation efficiency of *RB1* mRNA by performing a RIP (RNA-binding protein immunoprecipitation) assay against the translation initiation factor eIF4E. The relative translation efficiency is calculated by dividing the bound fraction of *RB1* with the bound fraction of housekeeping genes (*Actin* and *GAPDH*). Using this method, we found the relative translation efficiency of *RB1* was similar in sorted G1 and S/G2 cells as well as in asynchronously dividing and G1 arrested cells (Palbociclib treatment) (Fig. 1E, Fig. S1E). Taken together, our data indicate that Rb synthesis is not primarily responsible for its cell cycle dynamics.

Having found that Rb's cell cycle dynamics were not primarily due to transcription or translation mechanisms, we next sought to test if degradation mechanisms were responsible. To do this, we utilized a doxycyclin (Dox)-inducible system in which cells conditionally express Clover-3xFlag-tagged Rb (*TRE-Clover-3xFlag-Rb*) or Clover-NLS (*TRE-Clover-NLS*) upon Dox treatment (1µg/mL). After 36h of Dox treatment, we withdrew Dox and monitored the decrease of the Clover fluorescence signal using live cell imaging (Fig. S1F). Since the cells also express a FUCCI cell cycle marker, we can separately assess protein degradation taking place in G1 and S/G2 phases of the cell cycle (Fig. 1F, Fig. S1F). By fitting the degradation traces using a simple exponential decay function, we obtained the half-life of Clover-3xFlag-Rb protein in different cell cycle phases for each cell. Rb half-life in early G1 (median 6.4h; 75% range 5.3h-9.4h) is significantly shorter than it is in S/G2 (median 37.3h, 75% range 29.2h-45.4h) (Fig. 1F). The Rb

tag location does not affect its half-life since a C-terminally tagged Rb protein (Rb-3xFlag-Clover) behaved similarly to the N-terminally tagged version (Fig. 1G). The changing Rb stability through the cell cycle was specific to Rb since a short-lived Clover-NLS protein and stable Clover-NLS protein both had half-lives that did not change through the cell cycle (Fig. 1G; Fig. S1G, H). Thus, these results suggest a model where the Rb protein's cell cycle dynamics are due to its degradation in G1 and stabilization at the G1/S transition.

Having established that the regulation of Rb stability is most likely responsible for its cell cycle dynamics, we sought to test if this differential degradation of Rb is sufficient to give rise to the observed dynamics. To do this, we generated a mathematical model where only the half-life of the Rb protein changed through the cell cycle, while the synthesis rate remained constant (see methods). This simple model revealed that regulated degradation was sufficient to generate the cell-cycle dependent Rb concentration dynamics we observed, while the modest upregulation in the synthesis rate was insufficient (Fig. 1H). Thus, our findings imply that cell cycle-dependent regulation of Rb stability is responsible for its cell cycle dynamics (Fig. 1I).

Rb is stabilized via phosphorylation by Cdk

Having found that Rb is stabilized at the G1/S transition, we next sought to identify the molecular mechanism. One of the most prominent molecular changes occurring at the G1/S transition is the phosphorylation of Rb by cyclin-Cdk complexes. We therefore sought to examine how Rb phosphorylation affected its half-life. To do this, we first stained asynchronous HMEC cells with phospho-Rb (S807/811) and total Rb antibodies. We then calculated the Rb concentration in the low phospho-Rb G1 population (low pRb G1), the high phospho-Rb G1 population (high pRb G1), and the S/G2 population. The Rb concentration is lower in early G1 when it is not hyper-phosphorylated and then begins to recover in late G1, when Rb is phosphorylated (Fig. 2A). Similar results were obtained when G1 was partitioned into early and late phases using a live-cell Cdk activity sensor based on the C-terminal part of Rb (*17*) (Fig. S2A). These immunofluorescence data support the model where the Rb concentration decrease in G1 phase is reversed upon its phosphorylation. Consistently, when cells are arrested in G1 by treating them with the Cdk4/6 inhibitor Palbociclib (1μM) for 24 hours, the Rb protein concentration drops by ~75% (Fig. 2B) even though the mRNA concentration is only reduced by ~15% (Fig. S2B). This is consistent with published results showing significant Rb protein drops when cells are exposed to Cdk4/6 inhibitors(*18*). Furthermore, in cells expressing a Dox-inducible Clover-3xFlag-Rb protein, Palbociclib treatment led to a significant decrease in the concentration of this ectopically expressed protein but not the corresponding mRNA (Fig. S2C). Taken together, these data suggest that the phosphorylation of Rb by Cdk mediates its stabilization.

To further investigate how Rb phosphorylation on different Cdk phosphorylation sites affect its half-life, we used the Dox-inducible system to express a series of Rb variants in which the Cdk phosphorylation sites were either substituted with non-phosphorylatable alanines or with phospho-mimetic double glutamic acid residues (EE) (*19*) (Fig. S2D). For both mutant series, we extended the number of mutant sites from either the N- or C-terminus so that different mutants covered different parts of the protein (Fig. S2D). If Cdk phosphorylation stabilizes Rb, then the phospho-mutants (S/T to A) should exhibit a reduced half-life in S/G2, and the phospho-mimetic mutants (S/TP to EE) should exhibit increased half-life in early G1. Our results are consistent with this hypothesis (Fig. 2C, D; Fig. S2E, F). It is worth noting that the C-terminal alanine-mutants also had a more severe cell cycle arrest phenotype (Fig. S3A). This is likely because the alanine mutants do not allow the phosphorylation of C-terminal residues to disrupt Rb's interaction with E2F-DP (*12*, *17*, *20*, *21*). On the other hand, the phospho-mimetic mutants did not demonstrate significant cell cycle defects (Fig. S3B), likely because these Rb mutants are partially or entirely unable to bind and inhibit E2F. In addition, the introduction of phospho-mimetic mutations resulted in a smaller Rb concentration decrease in cells arrested in G1 using Palbociclib (Fig. S2C; Fig. S3C, D).

Interestingly, our mutational analysis did not reveal any particular phosphorylation sites that predominantly regulated Rb's half-life (Fig. 2E, F; Fig. S2F; Fig. S3C, D). Instead, the degree of Rb stabilization – *i.e.*, the ratio between early G1 and S/G2 half-lives – correlated with the total number of phospho-mimetic sites. This shows that many different phosphorylation sites contribute to Rb stability. We note that Rb14EE exhibited reduced half-lives for both early G1 and S/G2 phases, which is likely due to the additional SP230EE mutation destabilizing the protein via another mechanism. However, the difference between early G1 and S/G2 half-lives in Rb14EE is the smallest (Fig. S2F). Collectively, these results support the hypothesis that hyper-phosphorylation by Cdk stabilizes Rb in late G1 (Fig. 2G).

The degradation of un-phosphorylated Rb is mediated by the E3 ubiquitin ligase UBR5

After establishing that Rb is stabilized by phosphorylation at the G1/S transition, we next sought to identify the underlying molecular mechanism. To do this, we first tested whether Rb is degraded through the ubiquitin-proteasome system by treating cells with three commonly used inhibitors of different components of this degradation system: Bortezomib inhibits the proteasome; TAK243 inhibits the ubiquitin activating enzyme (E1); and MLN4924 inhibits the NEDD8-activating enzyme that activates the Cullin (CUL)-RING E3 ubiquitin ligases (*22*, *23*). We treated asynchronously growing HMEC cells with these inhibitors for 5 hours, and then immunostained the cells using antibodies for pRb(S807/811) and total Rb. TAK243 and Bortezomib treatments increased the Rb concentration in the low pRb G1 populations to a level similar to that in the high pRb G1 population, but MLN4924 did not (Fig. 3A, Fig. S4A). RPE-1 cells (telomerase immortalized retinal pigment epithelium cells) behaved similarly to HMEC

cells in that only TAK243 and Bortezomib treatments increased the Rb concentration in the low pRb G1 population (Fig. S4B). To further confirm that the phosphorylation status determines Rb degradation through the ubiquitin-proteasome system, we treated cells that were induced to express un-phosphorylatable Rb (Clover-3xFlag-RbΔCDK) or phospho-mimetic Rb (Clover-3xFlag-Rb14EE) with the three degradation inhibitors discussed above. The concentration of RbΔCDK is elevated by TAK243 and Bortezomib, but not MLN4924, and the concentration of Rb14EE does not increase following treatment by any of the three inhibitors (Fig. 3B). We also confirmed the enhanced ubiquitination of RbΔCDK by pulling down Clover-3xFlag-RbΔCDK and blotting for ubiquitin. RbΔCDK was more ubiquitinated than WT Rb (Fig. S4C). Altogether, these data suggest that un-phosphorylated Rb is degraded in G1 through the ubiquitin-proteasome system, but not by the Cullin (CUL)-RING E3 ligases.

There have been several previous studies of Rb degradation mechanisms that have identified some E3 ligases (*18*, *24–31*). For example, MDM2 may mediate Rb degradation via its central acidic domain (*24*, *25*, *29*). The human papilloma virus (HPV) E7 protein can bind Rb and induce its degradation (*28*), which is mediated by protease cleavage at Lys810 (*26*). More recently, Cdk4/6 inhibition was found to promote Rb degradation through βTrCP1-mediated ubiquitination (*18*). To test if these E3 ligases were responsible for the observed cell cycle dynamics of Rb, we examined the effect of knocking them down on the concentration of un-phosphorylatable Rb (Clover-3xFlag-RbΔCDK) and phospho-mimetic Rb (Clover-3xFlag-Rb14EE). If an E3 were responsible for Rb's cell cycle dynamics, we would expect to see an increase in the concentration of Clover-3xFlag-RbΔCDK but not of Clover-3xFlag-Rb14EE. None of the knockdowns exhibited this predicted phenotype (Fig. S5A). Even through some of the knockdowns affected the overall Rb concentration, this effect was not specific for unphosphorylated Rb and therefore could not explain Rb's cell cycle dynamics. Similarly, we performed the same set of knockdowns in cells arrested in G1 using Palbociclib and did not find any specific increase in the concentrations of un- or hypo-phosphorylated Rb (Fig. S5B-G). This implies that there must be some additional E3 ligase responsible for the phosphorylation-dependent degradation of Rb.

To identify the E3 ligases mediating the degradation of un-phosphorylated Rb, we set up an siRNA screen. We used a customized siRNA library that included the previously published E3 ligases for Rb, some nuclear localized E3s (according to UniProt), and some additional genes predicted to be E3 ligases for Rb (http://ubibrowser.bio-it.cn/ubibrowser_v3/) (Fig. 3C). HMEC cells inducibly expressing Clover-3xFlag-RbΔCDK or Clover-3xFlag-Rb14EE were transfected with the siRNA library. 48 hours later, cells were fixed and imaged. The concentration of Clover-3xFlag-Rb variants was measured in each treatment and its fold change over non-transfected cells was calculated. As positive controls, we included the ubiquitin-proteasome system inhibitors TAK243 and Bortezomib. As expected, TAK243 and Bortezomib only increased the concentration of RbΔCDK but not Rb14EE (Fig. 3D; Fig. S6A, B). From this

screen, we only identified UBR5 as specifically targeting unphosphorylated Rb for degradation. UBR5 is a verified E3 ubiquitin ligase belonging to the HECT family known to play roles in transcription and the DNA damage response (*32–35*) (Fig. 3D; Fig. S6A, B). However, Rb has never been reported to be a substrate of UBR5.

To confirm that UBR5 is the main E3 ligase targeting un-phosphorylated Rb, we first performed another siRNA screen with a different siRNA library containing UBR5 and 16 other E3 genes from the first library as well as the rest of the nuclear localized E3 genes not included in the first screen. We also included several E1 and E2 genes (Fig. 3C). This second siRNA screen also only identified UBR5 (Fig. 3D; Fig. S6B-D). We then validated UBR5 as a hit using another two independent siRNAs against UBR5. Knockdown of UBR5 in HMEC cells led to the accumulation of un/hypo-phosphorylated Rb after Palbociclib treatment, as measured by both immunoblot and immunostaining (Fig. 3E-G; Fig. S7A). We also measured the half-life of Rb following UBR5 knockdown using live-cell imaging and found that Rb was degraded about twice as slowly in early G1, but not in S/G2, as compared to the control siRNA (Fig. 3H). Moreover, we examined the effect of knocking down UBR5 on HMEC cells expressing endogenously tagged Rb (*RB1-3xFLAG-Clover-sfGFP*)(*10*). Following *UBR5* knockdown, the concentration of Rb does not decrease in early G1, but is instead kept relatively constant (Fig. S7B). To further confirm that the degradation of un-phosphorylated Rb by UBR5 is not cell line or cell type specific, we also examined epithelial RPE-1 cells as well as HLF (primary human lung fibroblast) and T98G (glioblastoma-derived fibroblast-like) cells. All of them showed that UBR5 knockdown increased concentrations of un- and hypo-phosphorylated Rb in Palbociclib-treated cells (Fig. S7C-E).

To test if UBR5 mediated Rb degradation *in vivo*, we examined its effect in the mouse liver using the *Fah-/-* system(*36*, *37*). In the *Fah-/-* system, deletion of the *Fah* gene causes toxin accumulation in hepatocytes that will lead to hepatocyte death. Toxin accumulation can be prevented by treating mice with NTBC (2-(2-nitro-4-trifluoromethylbenzoyl)-1,3-cyclohexanedione)(*37*). When NTBC is withdrawn, cells expressing exogenous *Fah*, introduced by injecting *Fah*+ transposons, will clonally expand to repopulate the injured liver (*37*) (Fig. 3I). Importantly, other genetic elements, such as Cas9 and gRNA, can be added to the *Fah* transposon so that they are co-integrated into some hepatocyte genomes. To knock out *Ubr5* in some hepatocytes, we modified an *Fah* transposon plasmid (*38*) and delivered *Fah-P2A-Cas9-sgUbr5* or *Fah-P2A-Cas9-sgNT* (non-targeting) transposons and the SB100 transposase into *Fah−/−* mice via hydrodynamic transfection. 8 weeks after injection, when the liver was almost fully repopulated with *Fah*+ cells, we isolated the hepatocytes, plated them, and performed immunostaining or immunoblots (Fig. 3I). Consistent with the results from human cell lines, knocking out *Ubr5* increased Rb concentrations in mouse hepatocytes where Rb was not hyper-phosphorylated (low pRb) (Fig. 3J, Fig. S7F). The results from *Fah-/- in vivo* model further

supports our conclusion that the E3 ligase UBR5 targets un-phosphorylated Rb for degradation in G1 (Fig. 3K).

Our results here give insight into why previous studies reported other E3s targeting Rb. First, any E3 whose knockdown results in a cell cycle phenotype would be predicted to have an effect on Rb concentration. Second, after finding Rb dynamics were driven by the degradation of un- or hypo-phosphorylated Rb in G1 phase, we sought to find E3s that specifically targeted the un-phosphorylatable RbΔCDK protein, but not the phospho-mimetic Rb14EE protein. We did find a significant increase in both RbΔCDK and Rb14EE when the E3 MDM2 was knocked down, and possibly very modest effects when other reported E3s were knocked down (Fig. S5A; Fig. S6A). This suggests that these different E3s operate in different cell types or contexts, but are not responsible for Rb's cell cycle dynamics.

UBR5 and Cdk4/6 drive parallel pathways promoting the G1/S transition

It is becoming increasingly clear that there are two distinct pathways driving the G1/S transition that both operate through Rb. First, the canonical Cdk-phosphorylation pathway through which cyclin D-Cdk4/6 complexes phosphorylate and inhibit Rb, and second, the Rb-degradation pathway that drives down the concentration of Rb in G1 phase. One prediction from this parallel pathway model is that cells lacking the Rb-degradation pathway should be more sensitive to inhibition of the remaining Rb-phosphorylation pathway. We can now test this prediction because we identified UBR5 as the E3 ligase targeting un-phosphorylated Rb in G1. To do this, we first generated clonal cell lines lacking *UBR5* from HMEC cells using CRISPR/Cas9. We randomly picked three *UBR5 WT* clones and three *UBR5 KO* clones for analysis (Fig. 4A). *UBR5 KO* cells exhibited higher Rb concentrations in low pRb G1 cells (Fig. 4B, C; Fig. S8). Moreover, *UBR5 KO* cells also exhibited both higher endogenous Rb concentrations and higher exogenous Clover-3xFlag-Rb concentrations following Palbociclib treatment to arrest cells in G1 (Fig. S8; Fig. S9A, B), as well as an increased Rb half-life in early G1 (Fig. S9C). These knockout lines therefore exhibited all the same effects we observed in our earlier knockdown experiments shown in Fig. 3.

Having established *UBR5 KO* cells, we are now in a position to test the parallel pathway model prediction that cells lacking the Rb-degradation pathway are more sensitive to inhibition of the Rb-phosphorylation pathway. To do this, we treated *UBR5 WT* and *UBR5 KO* cells with the Cdk4/6 inhibitor Palbociclib for 72 hours and then measured cell numbers. Since different clonal cell lines had different proliferation rates to begin with (Fig. S10A), we normalized the cell numbers of Palbociclib treated cells to the cell numbers in the DMSO control treatment for each clonal cell line. Moreover, this normalization also accounts for the slower growth rates of *UBR5 KO* cells (Fig. S10A) that are likely due to the dysregulation of other UBR5 substrates. As predicted by the parallel pathway model, *UBR5 KO* cells are more sensitive to Palbociclib

treatment than *UBR5 WT* cells (Fig. 4D, Fig. S10A). To further determine the proliferation status of *UBR5 WT* and *KO* cells, we also stained the cells with phospho-Rb antibodies following DMSO or Palbociclib treatments. As expected, a significantly higher proportion of *UBR5 WT* cells were progressing through the cell cycle (as indicated by cells having hyper-phosphorylated Rb) compared to *UBR5 KO* cells, again supporting the parallel pathway model (Fig. S10B-D).

Since UBR5 has other substrates that may also affect cell cycle progression, we wanted to examine if UBR5 KO cells' increased sensitivity to Palbociclib treatment was due to the stabilization of Rb. To test this, we knocked out *RB1* in *UBR5 KO* cells using CRISPR/Cas9 (Fig. S11A) and tested their sensitivity to Palbociclib treatment. Knocking out *RB1* in *UBR5 KO* cells completely rescued the increased Palbociclib sensitivity exhibited by *UBR5 KO* cells (Fig. 4E; Fig. S11B), suggesting that the effect of UBR5 on the G1/S transition is primarily through the stabilization of Rb. Lastly, to make sure that the effect of UBR5 on cell cycle progression was due to its E3 ligase activity, we added back either wild-type UBR5 or an inactive mutant UBR5 to the *UBR5 KO* cells using the Dox-inducible system (Fig. S11C). The mutant UBR5 has a C2768A mutation in the HECT domain, which kills its catalytic activity (*33*). The expression of WT or mutant UBR5 was induced by Dox, and cells were treated with DMSO or Palbociclib for 72 hours. Adding back UBR5 WT increased the normalized cell number as compared to the no Dox control, whereas adding back the mutant UBR5 did not (Fig. 4F; Fig. S11D, E). This indicates that the E3 ligase activity of UBR5 is essential for its function as a key component of the Rb-degradation pathway driving progression through the G1/S transition.

Discussion

Two distinct pathways drive the G1/S transition by reducing the activity and amount of the key cell cycle inhibitor Rb: the canonical Cdk-phosphorylation pathway and the Rb-degradation pathway (Fig. 4G). Here, we report that the Rb-degradation pathway is driven by the E3 ubiquitin ligase UBR5 and is shut off by Rb hyper-phosphorylation in late G1. However, we do not yet know the mechanism through which UBR5 recognizes Rb. UBR5 likely engages its substrates as a dimer or tetramer, which can target distinct degron linear motifs as indicated by recent cryo-EM structures (*34*, *35*, *39–41*). Since UBR5 is a large multi-domain protein, it is possible that different docking mechanisms can be utilized for engaging different groups of substrates involved in multiple biological processes (*33*, *35*, *40–42*). Interestingly, two recent studies proposed that UBR5 targets its substrates on chromatin (*34*, *35*). This possible preference of UBR5 for chromatin-bound targets might explain the results of our mutational analysis of Rb. Namely, the more tightly an Rb variant is predicted to bind the E2F transcription factor, the more rapidly it is degraded. The stabilization of Rb at the G1/S transition is coincident with its hyper-phosphorylation and subsequent dissociation from the chromatin-bound E2F transcription factors.

Components of the canonical Rb-phosphorylation pathway are frequently mutated in cancer and have become targets for therapies (*43*). For example, Cdk4/6 inhibitors in combination with endocrine therapy are used to treat advanced estrogen receptor positive (ER+)/human epidermal growth factor receptor-2 negative (HER2-) breast cancers (*44–46*). However, this application is frequently limited by the intrinsic and acquired therapeutic resistance observed in patients (*47*, *48*). One possible way to improve upon current therapies targeting the Rb-phosphorylation pathway is to also target the Rb-degradation pathway. Namely, since deleting UBR5 sensitizes cells to treatment by Cdk4/6 inhibitors, it is possible that current Cdk4/6 inhibitor-based treatments for breast cancer can be improved by developing novel therapeutics targeting the Rb-degradation pathway through UBR5.

The inability of current therapies to inhibit cell division likely reflects our incomplete knowledge of the signaling pathways involved. During G1 phase, the cell integrates many signals to make tiehe decision to commit to cell division including two separate signaling pathways targeting Rb. The existence of these two parallel pathways explains the ability of some cells to proliferate in the absence of cyclin D-dependent kinase activity (*49–51*). Namely, these cells rely more heavily on the UBR5-Rb degradation pathway than the canonical Cdk4/6 Rb-phosphorylation pathway. In addition to providing such a robust entry to the cell division cycle in a particular cellular context, the existence of parallel pathways regulating the G1/S transition might be due to the different proliferative requirements of diverse cell types (*52*). Different pathways can be independently tuned to precisely calibrate the rate of proliferation required by the myriad cell types and niches of a multicellular organism. Discovering the mechanisms underlying these G1/S regulatory pathways, such as we have here for Rb-degradation, will give insight into both development and disease.

References

1. C. Schwarz, A. Johnson, M. Kõivomägi, E. Zatulovskiy, C. J. Kravitz, A. Doncic, J. M. Skotheim, A Precise Cdk Activity Threshold Determines Passage through the Restriction Point. *Mol Cell*. **69**, 253-264.e5 (2018).

2. S. D. Cappell, M. Chung, A. Jaimovich, S. L. Spencer, T. Meyer, Irreversible APCCdh1 Inactivation Underlies the Point of No Return for Cell-Cycle Entry. *Cell*. **166**, 167–180 (2016).

3. J. Moser, I. Miller, D. Carter, S. L. Spencer, Control of the Restriction Point by Rb and p21. *Proceedings of the National Academy of Sciences*. **115**, E8219–E8227 (2018).

4. A. Zetterberg, O. Larsson, K. G. Wiman, What is the restriction point? *Curr Opin Cell Biol*. **7**, 835–842 (1995).

5. S. M. Rubin, J. Sage, J. M. Skotheim, Integrating Old and New Paradigms of G1/S Control. *Mol Cell*. **80**, 183–192 (2020).

6. J. T. Winston, W. J. Pledger, Growth factor regulation of cyclin D1 mRNA expression through protein synthesis-dependent and -independent mechanisms. *Mol Biol Cell*. **4**, 1133–1144 (1993).

7. A. Fassl, Y. Geng, P. Sicinski, CDK4 and CDK6 kinases: From basic science to cancer therapy. *Science*. **375**, eabc1495 (2022).

8. A. M. Narasimha, M. Kaulich, G. S. Shapiro, Y. J. Choi, P. Sicinski, S. F. Dowdy, Cyclin D activates the Rb tumor suppressor by mono-phosphorylation. *eLife*. **3**, e02872 (2014).

9. I. Sanidas, R. Morris, K. A. Fella, P. H. Rumde, M. Boukhali, E. C. Tai, D. T. Ting, M. S. Lawrence, W. Haas, N. J. Dyson, A Code of Mono-phosphorylation Modulates the Function of RB. *Mol Cell*. **73**, 985-1000.e6 (2019).

10. E. Zatulovskiy, S. Zhang, D. F. Berenson, B. R. Topacio, J. M. Skotheim, Cell growth dilutes the cell cycle inhibitor Rb to trigger cell division. *Science*. **369**, 466–471 (2020).

11. S. Zhang, E. Zatulovskiy, J. Arand, J. Sage, J. M. Skotheim, The cell cycle inhibitor RB is diluted in G1 and contributes to controlling cell size in the mouse liver (2022), p. 2022.06.08.495371, , doi:10.1101/2022.06.08.495371.

12. B. R. Topacio, E. Zatulovskiy, S. Cristea, S. Xie, C. S. Tambo, S. M. Rubin, J. Sage, M. Kõivomägi, J. M. Skotheim, Cyclin D-Cdk4,6 Drives Cell-Cycle Progression via the Retinoblastoma Protein's C-Terminal Helix. *Mol Cell*. **74**, 758-770.e4 (2019).

13. S. L. Spencer, S. D. Cappell, F.-C. Tsai, K. W. Overton, C. L. Wang, T. Meyer, The proliferation-quiescence decision is controlled by a bifurcation in CDK2 activity at mitotic exit. *Cell*. **155**, 369–383 (2013).

14. M. C. Lanz, E. Zatulovskiy, M. P. Swaffer, L. Zhang, I. Ilerten, S. Zhang, D. S. You, G. Marinov, P. McAlpine, J. E. Elias, J. M. Skotheim, Increasing cell size remodels the proteome and promotes senescence (2021), p. 2021.07.29.454227, , doi:10.1101/2021.07.29.454227.

15. A. Sakaue-Sawano, H. Kurokawa, T. Morimura, A. Hanyu, H. Hama, H. Osawa, S. Kashiwagi, K. Fukami, T. Miyata, H. Miyoshi, T. Imamura, M. Ogawa, H. Masai, A. Miyawaki, Visualizing Spatiotemporal Dynamics of Multicellular Cell-Cycle Progression. *Cell*. **132**, 487–498 (2008).

16. C. Xia, J. Fan, G. Emanuel, J. Hao, X. Zhuang, Spatial transcriptome profiling by MERFISH reveals subcellular RNA compartmentalization and cell cycle-dependent gene expression. *Proceedings of the National Academy of Sciences*. **116**, 19490–19499 (2019).

17. J. R. Burke, T. J. Liban, T. Restrepo, H.-W. Lee, S. M. Rubin, Multiple Mechanisms for E2F Binding Inhibition by Phosphorylation of the Retinoblastoma Protein C-Terminal Domain. *Journal of Molecular Biology*. **426**, 245–255 (2014).

18. F. Dang, L. Nie, J. Zhou, K. Shimizu, C. Chu, Z. Wu, A. Fassl, S. Ke, Y. Wang, J. Zhang, T. Zhang, Z. Tu, H. Inuzuka, P. Sicinski, A. J. Bass, W. Wei, Inhibition of CK1ε potentiates the therapeutic efficacy of CDK4/6 inhibitor in breast cancer. *Nat Commun*. **12**, 5386 (2021).

19. M. V. Repetto, M. J. Winters, A. Bush, W. Reiter, D. M. Hollenstein, G. Ammerer, P. M. Pryciak, A. Colman-Lerner, CDK and MAPK Synergistically Regulate Signaling Dynamics via a Shared Multi-site Phosphorylation Region on the Scaffold Protein Ste5. *Molecular Cell*. **69**, 938-952.e6 (2018).

20. E. S. Knudsen, J. Y. Wang, Dual mechanisms for the inhibition of E2F binding to RB by cyclin-dependent kinase-mediated RB phosphorylation. *Mol Cell Biol*. **17**, 5771–5783 (1997).

21. V. D. Brown, R. A. Phillips, B. L. Gallie, Cumulative Effect of Phosphorylation of pRB on Regulation of E2F Activity. *Mol Cell Biol*. **19**, 3246–3256 (1999).

22. R. J. Deshaies, E. D. Emberley, A. Saha, Control of cullin-ring ubiquitin ligase activity by nedd8. *Subcell Biochem*. **54**, 41–56 (2010).

23. Z. Luo, Y. Pan, L. S. Jeong, J. Liu, L. Jia, Inactivation of the Cullin (CUL)-RING E3 ligase by the NEDD8-activating enzyme inhibitor MLN4924 triggers protective autophagy in cancer cells. *Autophagy*. **8**, 1677–1679 (2012).

24. P. Sdek, H. Ying, H. Zheng, A. Margulis, X. Tang, K. Tian, Z.-X. J. Xiao, The central acidic domain of MDM2 is critical in inhibition of retinoblastoma-mediated suppression of E2F and cell growth. *J Biol Chem*. **279**, 53317–53322 (2004).

25. P. Sdek, H. Ying, D. L. F. Chang, W. Qiu, H. Zheng, R. Touitou, M. J. Allday, Z.-X. J. Xiao, MDM2 Promotes Proteasome-Dependent Ubiquitin-Independent Degradation of Retinoblastoma Protein. *Molecular Cell*. **20**, 699–708 (2005).

26. T. Tomita, J. M. Huibregtse, A. Matouschek, A masked initiation region in retinoblastoma protein regulates its proteasomal degradation. *Nat Commun*. **11**, 2019 (2020).

27. Y. Wang, Z. Zheng, J. Zhang, Y. Wang, R. Kong, J. Liu, Y. Zhang, H. Deng, X. Du, Y. Ke, A Novel Retinoblastoma Protein (RB) E3 Ubiquitin Ligase (NRBE3) Promotes RB Degradation and Is Transcriptionally Regulated by E2F1 Transcription Factor *. *Journal of Biological Chemistry*. **290**, 28200–28213 (2015).

28. S. N. Boyer, D. E. Wazer, V. Band, E7 Protein of Human Papilloma Virus-16 Induces Degradation of Retinoblastoma Protein through the Ubiquitin-Proteasome Pathway1. *Cancer Research*. **56**, 4620–4624 (1996).

29. C. Uchida, S. Miwa, K. Kitagawa, T. Hattori, T. Isobe, S. Otani, T. Oda, H. Sugimura, T. Kamijo, K. Ookawa, H. Yasuda, M. Kitagawa, Enhanced Mdm2 activity inhibits pRB function via ubiquitin-dependent degradation. *EMBO J*. **24**, 160–169 (2005).

30. H. Liu, J. Wang, Y. Liu, L. Hu, C. Zhang, B. Xing, X. Du, Human U3 protein14a is a novel type ubiquitin ligase that binds RB and promotes RB degradation depending on a leucine-rich region. *Biochimica et Biophysica Acta (BBA) - Molecular Cell Research*. **1865**, 1611–1620 (2018).

31. E. Sun, P. Zhang, RNF12 Promotes Glioblastoma Malignant Proliferation via Destructing RB1 and Regulating MAPK Pathway. *J Healthc Eng*. **2021**, 4711232 (2021).

32. A. de Vivo, A. Sanchez, J. Yegres, J. Kim, S. Emly, Y. Kee, The OTUD5–UBR5 complex regulates FACT-mediated transcription at damaged chromatin. *Nucleic Acids Research*. **47**, 729–746 (2019).

33. T. Gudjonsson, M. Altmeyer, V. Savic, L. Toledo, C. Dinant, M. Grøfte, J. Bartkova, M. Poulsen, Y. Oka, S. Bekker-Jensen, N. Mailand, B. Neumann, J.-K. Heriche, R. Shearer, D. Saunders, J. Bartek, J. Lukas, C. Lukas, TRIP12 and UBR5 Suppress Spreading of Chromatin Ubiquitylation at Damaged Chromosomes. *Cell*. **150**, 697–709 (2012).

34. J. M. Tsai, J. D. Aguirre, Y.-D. Li, J. Brown, V. Focht, L. Kater, G. Kempf, B. Sandoval, S. Schmitt, J. C. Rutter, P. Galli, C. R. Sandate, J. A. Cutler, C. Zou, K. A. Donovan, R. J. Lumpkin, S. Cavadini, P. M. C. Park, Q. Sievers, C. Hatton, E. Ener, B. D. Regalado, M. T. Sperling, M. Słabicki, J. Kim, R. Zon, Z. Zhang, P. G. Miller, R. Belizaire, A. S. Sperling, E. S. Fischer, R. Irizarry, S. A. Armstrong, N. H. Thomä, B. L. Ebert, UBR5 forms ligand-dependent complexes on chromatin to regulate nuclear hormone receptor stability. *Molecular Cell*. **0** (2023), doi:10.1016/j.molcel.2023.06.028.

35. K. G. Mark, S. Kolla, J. D. Aguirre, D. M. Garshott, S. Schmitt, D. L. Haakonsen, C. Xu, L. Kater, G. Kempf, B. Martínez-González, D. Akopian, S. K. See, N. H. Thomä, M. Rapé,

475 Orphan quality control shapes network dynamics and gene expression. *Cell*. **0** (2023),
476 doi:10.1016/j.cell.2023.06.015.

477 36. H. Azuma, N. Paulk, A. Ranade, C. Dorrell, M. Al-Dhalimy, E. Ellis, S. Strom, M. A. Kay,
478 M. Finegold, M. Grompe, Robust expansion of human hepatocytes in Fah-/-/Rag2-/-/Il2rg-
479 /- mice. *Nat Biotechnol*. **25**, 903–910 (2007).

480 37. M. Grompe, Fah Knockout Animals as Models for Therapeutic Liver Repopulation. *Adv Exp*
481 *Med Biol*. **959**, 215–230 (2017).

482 38. M. Zhu, T. Lu, Y. Jia, X. Luo, P. Gopal, L. Li, M. Odewole, V. Renteria, A. G. Singal, Y.
483 Jang, K. Ge, S. C. Wang, M. Sorouri, J. R. Parekh, M. P. MacConmara, A. C. Yopp, T.
484 Wang, H. Zhu, Somatic Mutations Increase Hepatic Clonal Fitness and Regeneration in
485 Chronic Liver Disease. *Cell*. **177**, 608-621.e12 (2019).

486 39. L. A. Hehl, D. Horn-Ghetko, J. R. Prabu, R. Vollrath, D. T. Vu, D. A. P. Berrocal, M. P. C.
487 Mulder, G. J. van der H. van Noort, B. A. Schulman, Structural snapshots along K48-linked
488 ubiquitin chain formation by the HECT E3 UBR5 (2023), p. 2023.06.06.543850, ,
489 doi:10.1101/2023.06.06.543850.

490 40. Z. Hodáková, I. Grishkovskaya, H. L. Brunner, D. L. Bolhuis, K. Belačić, A. Schleiffer, H.
491 Kotisch, N. G. Brown, D. Haselbach, Cryo-EM structure of the chain-elongating E3 ligase
492 UBR5 (2022), p. 2022.11.03.515015, , doi:10.1101/2022.11.03.515015.

493 41. F. Wang, Q. He, W. Zhan, Z. Yu, E. Finkin-Groner, X. Ma, G. Lin, H. Li, Structure of the
494 human UBR5 E3 ubiquitin ligase. *Structure*. **31**, 541-552.e4 (2023).

495 42. W. Jiang, S. Wang, M. Xiao, Y. Lin, L. Zhou, Q. Lei, Y. Xiong, K.-L. Guan, S. Zhao,
496 Acetylation regulates gluconeogenesis by promoting PEPCK1 degradation via recruiting
497 the UBR5 ubiquitin ligase. *Mol Cell*. **43**, 33–44 (2011).

498 43. J. M. Suski, M. Braun, V. Strmiska, P. Sicinski, Targeting cell-cycle machinery in cancer.
499 *Cancer Cell*. **39**, 759–778 (2021).

500 44. R. S. Finn, M. Martin, H. S. Rugo, S. Jones, S.-A. Im, K. Gelmon, N. Harbeck, O. N.
501 Lipatov, J. M. Walshe, S. Moulder, E. Gauthier, D. R. Lu, S. Randolph, V. Diéras, D. J.
502 Slamon, Palbociclib and Letrozole in Advanced Breast Cancer. *New England Journal of*
503 *Medicine*. **375**, 1925–1936 (2016).

504 45. G. N. Hortobagyi, S. M. Stemmer, H. A. Burris, Y.-S. Yap, G. S. Sonke, S. Paluch-Shimon,
505 M. Campone, K. L. Blackwell, F. André, E. P. Winer, W. Janni, S. Verma, P. Conte, C. L.
506 Arteaga, D. A. Cameron, K. Petrakova, L. L. Hart, C. Villanueva, A. Chan, E. Jakobsen, A.
507 Nusch, O. Burdaeva, E.-M. Grischke, E. Alba, E. Wist, N. Marschner, A. M. Favret, D.
508 Yardley, T. Bachelot, L.-M. Tseng, S. Blau, F. Xuan, F. Souami, M. Miller, C. Germa, S.
509 Hirawat, J. O'Shaughnessy, Ribociclib as First-Line Therapy for HR-Positive, Advanced
510 Breast Cancer. *N Engl J Med*. **375**, 1738–1748 (2016).

46. C. J. Sherr, D. Beach, G. I. Shapiro, Targeting CDK4 and CDK6: From Discovery to Therapy. *Cancer Discovery*. **6**, 353–367 (2016).

47. A. C. Garrido-Castro, S. Goel, CDK4/6 Inhibition in Breast Cancer: Mechanisms of Response and Treatment Failure. *Curr Breast Cancer Rep*. **9**, 26–33 (2017).

48. L. M. Spring, S. A. Wander, F. Andre, B. Moy, N. C. Turner, A. Bardia, Cyclin-dependent kinase 4 and 6 inhibitors for hormone receptor-positive breast cancer: past, present, and future. *The Lancet*. **395**, 817–827 (2020).

49. M. Malumbres, R. Sotillo, D. Santamaría, J. Galán, A. Cerezo, S. Ortega, P. Dubus, M. Barbacid, Mammalian cells cycle without the D-type cyclin-dependent kinases Cdk4 and Cdk6. *Cell*. **118**, 493–504 (2004).

50. K. Kozar, M. A. Ciemerych, V. I. Rebel, H. Shigematsu, A. Zagozdzon, E. Sicinska, Y. Geng, Q. Yu, S. Bhattacharya, R. T. Bronson, K. Akashi, P. Sicinski, Mouse development and cell proliferation in the absence of D-cyclins. *Cell*. **118**, 477–491 (2004).

51. C. Liu, Y. Konagaya, M. Chung, L. H. Daigh, Y. Fan, H. W. Yang, K. Terai, M. Matsuda, T. Meyer, Altered G1 signaling order and commitment point in cells proliferating without CDK4/6 activity. *Nat Commun*. **11**, 5305 (2020).

52. A. Regev, S. A. Teichmann, E. S. Lander, I. Amit, C. Benoist, E. Birney, B. Bodenmiller, P. Campbell, P. Carninci, M. Clatworthy, H. Clevers, B. Deplancke, I. Dunham, J. Eberwine, R. Eils, W. Enard, A. Farmer, L. Fugger, B. Göttgens, N. Hacohen, M. Haniffa, M. Hemberg, S. Kim, P. Klenerman, A. Kriegstein, E. Lein, S. Linnarsson, E. Lundberg, J. Lundeberg, P. Majumder, J. C. Marioni, M. Merad, M. Mhlanga, M. Nawijn, M. Netea, G. Nolan, D. Pe'er, A. Phillipakis, C. P. Ponting, S. Quake, W. Reik, O. Rozenblatt-Rosen, J. Sanes, R. Satija, T. N. Schumacher, A. Shalek, E. Shapiro, P. Sharma, J. W. Shin, O. Stegle, M. Stratton, M. J. T. Stubbington, F. J. Theis, M. Uhlen, A. van Oudenaarden, A. Wagner, F. Watt, J. Weissman, B. Wold, R. Xavier, N. Yosef, Human Cell Atlas Meeting Participants, The Human Cell Atlas. *eLife*. **6**, e27041 (2017).

53. K. J. Abraham, N. Khosraviani, J. N. Y. Chan, A. Gorthi, A. Samman, D. Y. Zhao, M. Wang, M. Bokros, E. Vidya, L. A. Ostrowski, R. Oshidari, V. Pietrobon, P. S. Patel, A. Algouneh, R. Singhania, Y. Liu, V. T. Yerlici, D. D. De Carvalho, M. Ohh, B. C. Dickson, R. Hakem, J. F. Greenblatt, S. Lee, A. J. R. Bishop, K. Mekhail, Nucleolar RNA polymerase II drives ribosome biogenesis. *Nature*. **585**, 298–302 (2020).

54. M. Charni-Natan, I. Goldstein, Protocol for Primary Mouse Hepatocyte Isolation. *STAR Protoc*. **1**, 100086 (2020).

55. Y. Jin, T. Anbarchian, P. Wu, A. Sarkar, M. Fish, W. C. Peng, R. Nusse, Wnt signaling regulates hepatocyte cell division by a transcriptional repressor cascade. *Proceedings of the National Academy of Sciences*. **119**, e2203849119 (2022).

56. D. F. Berenson, E. Zatulovskiy, S. Xie, J. M. Skotheim, Constitutive expression of a fluorescent protein reports the size of live human cells. *MBoC*. **30**, 2985–2995 (2019).

549 57. C. Lucchesi, S. Mohibi, X. Chen, Measuring Translation Efficiency by RNA
550 Immunoprecipitation of Translation Initiation Factors. *Methods Mol Biol*. **2267**, 73–79
551 (2021).

552 58. X. Liu, J. Yan, M. W. Kirschner, Beyond G1/S regulation: how cell size homeostasis is
553 tightly controlled throughout the cell cycle? (2022), p. 2022.02.03.478996, ,
554 doi:10.1101/2022.02.03.478996.

555
556
557

Acknowledgements

We thank Julien Sage, Seth Rubin, Hao Zhu, Peter Pryciak and members of the Skotheim laboratory for discussions and feedback on the manuscript. We thank Hao Zhu for sharing the *Fah* transposon plasmids. We thank Markus Grompe for sharing the *Fah-/-* mice. This work was supported by a Chan Zuckerberg Biohub Investigator Award (J.M.S.), and the NIH (P01 CA254867 and K99GM147351). The siRNA screens were done using the ImageXpress Micro CONFOCAL microscope at the High Throughput Screening Knowledge Center (HTSKC) at Stanford, which was funded by the NIH Shared Instrumentation Grant (S10OD026899).

Author contributions

S.Z. performed the experiments, L.V. performed the mathematical modeling, E.Z., S.Z, and J.M.S. designed the experiments, and S.Z. and J.M.S. wrote the manuscript.

Competing interests

The authors declare no competing interest.

Supplementary Materials

Materials and Methods

Figs. S1 to S11

Table S1

Figures and Figure captions

Fig. 1

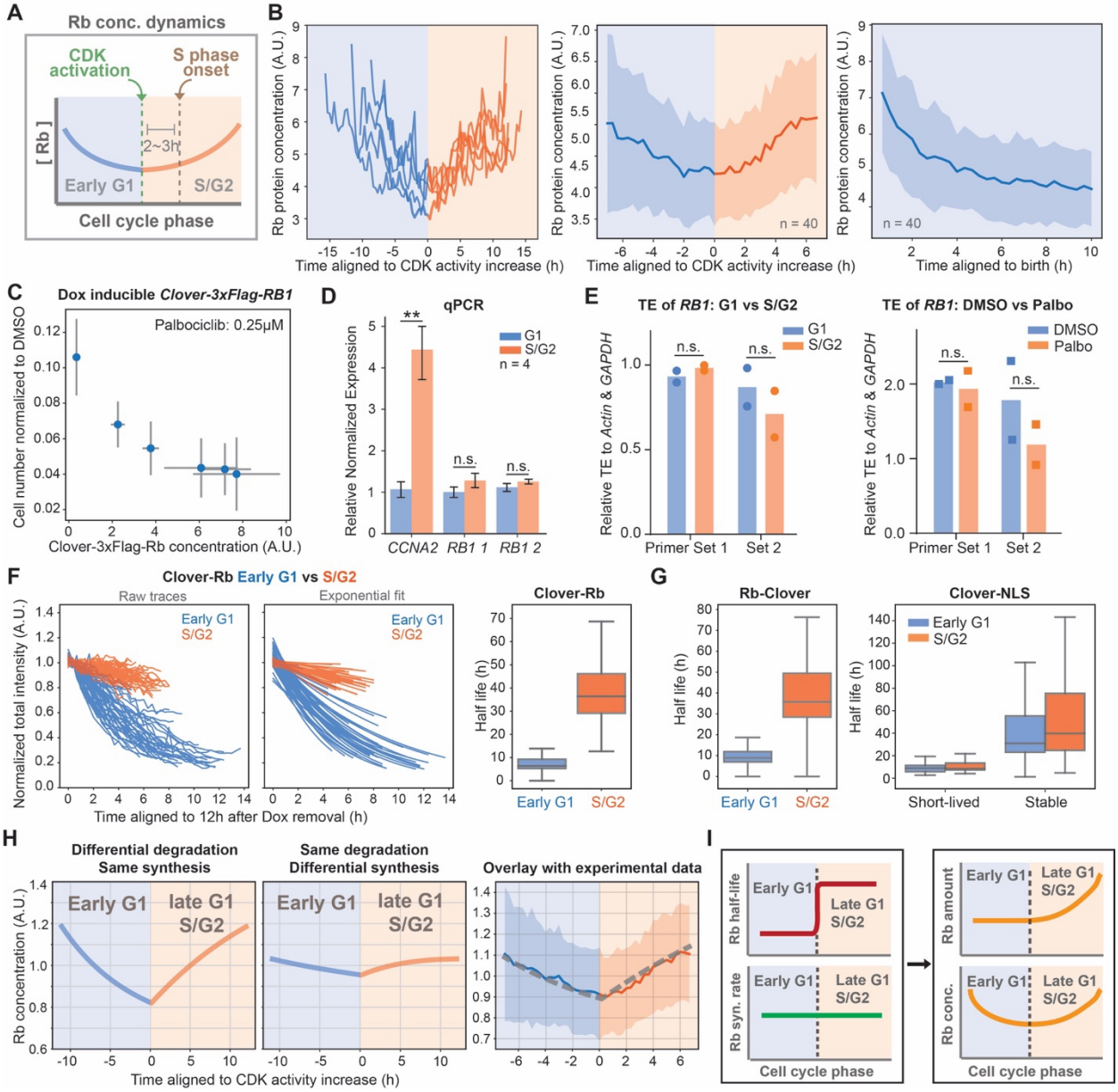

Fig. 1. Rb concentration dynamics are determined by degradation in early- to mid-G1
A. Schematic illustration of Rb concentration dynamics through the cell cycle. CDK activation occurs 2-3 hours before the initiation of DNA replication (*1*, *10*). **B**. Fluorescent traces from HMEC-hTERT1 cells expressing endogenously tagged *RB1-3xFLAG-Clover-sfGFP* and the HDHB CDK sensor [1] (n = 40). Left panel shows representative single-cell traces and the middle and right panels show average traces with shaded regions indicating the standard deviation. Traces are aligned either by the initial translocation of the HDHB CDK sensor (middle panel) or cell birth (right panel). **C.** Normalized cell number of HMEC cells treated with either DMSO or Palbociclib (0.25μM) for 72 hours. Cells were plated in media containing different doses of doxycycline to induce exogenous Clover-3xFlag-Rb. Drug treatment started the next day and lasted for 72 hours. Then, cells were fixed and the cell number in each well was measured. Normalized cell number is the cell number under Palbociclib treatment divided by the cell number under DMSO treatment. N = 3 biological replicates, the error bar indicates standard deviation. **D.** qPCR (n = 4) measurements of the *RB1* mRNA concentration in G1 and S/G2 HMEC cells sorted using a FUCCI cell cycle reporter. **E.** Translation efficiency (TE) of *RB1* was determined in HMEC cells in G1 and S/G2 that had been sorted using a FUCCI marker (left panel), and in HMEC cells treated with DMSO or Palbociclib (1μM) (right panel). TE was measured using a RIP assay (RNA binding protein immunoprecipitation) by pulling down eIF4E. TE is calculated by dividing the eIF4E bound fraction of *RB1* mRNA to the eIF4E bound fraction of *GAPDH & Actin* mRNAs. Bars denote mean values and dots denote each replicate experiment. **F.** (Left panel) The degradation traces of Clover-3xFlag-Rb protein after Dox withdrawal. The traces were classified into early G1 phase or S/G2 phase based on a FUCCI cell cycle marker and cell cycle phase duration. (Middle panel) The exponential fit of the degradation traces. (Right panel) Distribution of half-lives estimated from the exponential fit. Box plot indicates 5th, 25th, median, 75th and 95th percentiles. **G.** Same half-life measurement as in panel F, but using a C-terminally tagged Rb-3xFlag-Clover (Left panel) or a short-lived Clover-NLS or stable Clover-NLS (Right panel). **H.** Mathematical model of Rb concentration dynamics during cell cycle progression (see methods). Left panel: Rb concentration dynamics assuming that its degradation rate decreases by 80% at the G1/S transition as measured by live imaging (see panel F) and its synthesis rate does not change (left panel), or if Rb's degradation rate does not change, but its synthesis rate increases by 20% at the G1/S transition as measured in panel D. Right panel shows the overlay of the model based on regulated Rb degradation with the experimental data from panel B (middle panel). Rb concentration is normalized to the mean. **I.** Model schematic: differential degradation of Rb in G1 and S/G2 phases of the cell cycle drive its concentration dynamics.

Fig. 2

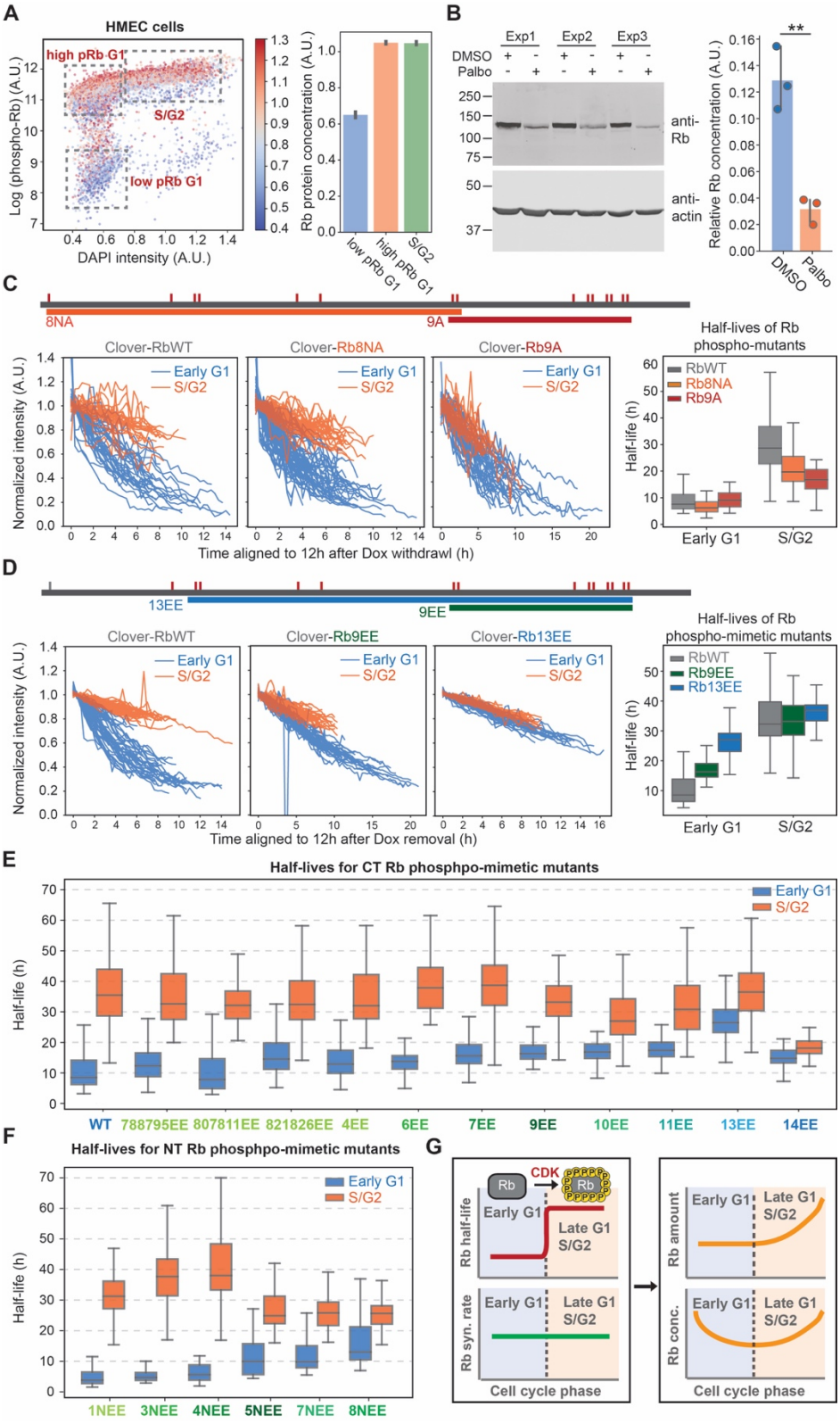

Fig. 2. Rb protein is stabilized via phosphorylation by Cyclin-Cdk

A. Rb concentration in different phospho-Rb populations. HMEC cells were stained with phospho-Rb (S807/811) antibody and Rb antibody. (Left panel) phospho-Rb intensity is plotted against DNA content (DAPI intensity). The color indicates Rb concentration. (Right panel) quantification Rb concentrations in different phospho-Rb populations as shown in the boxes in the left panel. Bar plots indicate the mean and 95% confidence interval. **B.** Immunoblot of Rb after DMSO or Palbociclib (1μM) treatment for 24 hours. The quantification of relative Rb concentration (normalized to actin intensity) is shown on the right. **C.** Top panel shows the schematic of Rb phospho-site mutants. Small red lines indicate the location of Cdk phosphorylation sites. Lower panel shows the degradation traces for Clover-3xFlag-RbWT, Clover-3xFlag-Rb8NA, and Clover-3xFlag-Rb9A as well as the corresponding distributions of half-lives. **D.** Top panel shows the schematic of the Rb phospho-mimetic mutants. Lower panel shows the degradation traces for Clover-3xFlag-RbWT, Clover-3xFlag-Rb9EE, and Clover-3xFlag-Rb13EE, as well as the corresponding distributions of half-lives. **E-F.** Half-life distributions for all the Rb phospho-mimetic mutants. **G.** Model schematic: Rb is stabilized in late G1 and S/G2 phases by Cdk phosphorylation.

644 **Fig. 3**

645

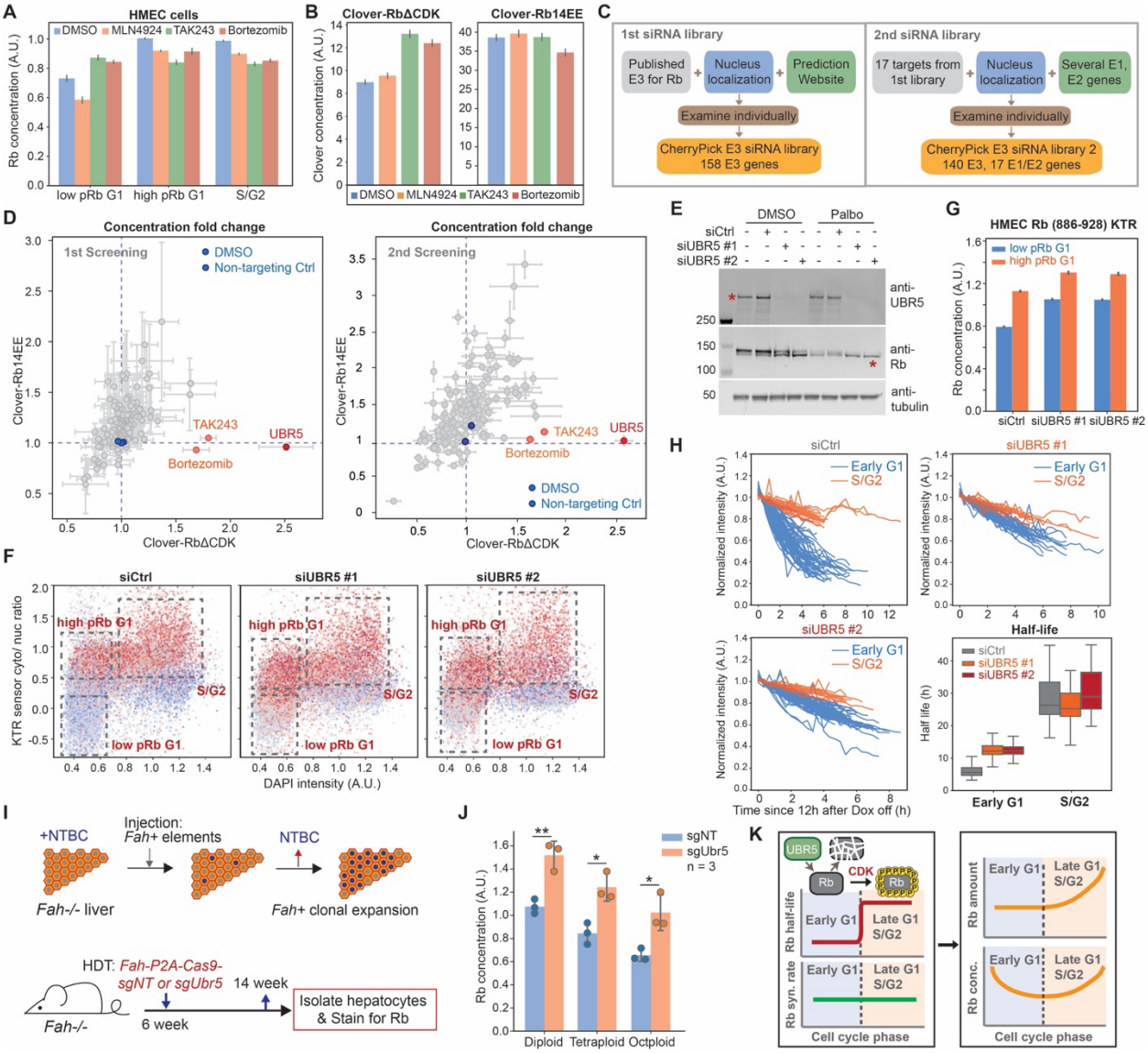

646

647

648

Fig. 3. The degradation of un-phosphorylated Rb is mediated by the E3 ligase UBR5

A. Rb concentration in different phospho-Rb populations of HMEC cells after indicated drug treatments. HMEC cells were treated with the indicated drugs for 5 hours, fixed, and stained with phospho-Rb (S807/811) and Rb antibodies. The Rb concentration is calculated by dividing total Rb intensity by nuclear area$^{3/2}$. **B.** Concentrations of Clover-3xFlag-RbΔCDK or Clover-3xFlag-Rb14EE after drug treatments. Cells expressing Clover-3xFlag-RbΔCDK and Clover-3xFlag-Rb14EE were induced with Dox (1μg/mL) for 48 hours. Then, cells were treated with the indicated drugs for 5 hours, fixed, and imaged. The concentrations of Clover-3xFlag-Rb variants were calculated by dividing total Clover intensity by nuclear area$^{3/2}$. **C.** Schematics of the two siRNA library components. **D.** Results of the two siRNA screens. The concentration fold changes of Clover-3xFlag-RbΔCDK and Clover-3xFlag-Rb14EE are plotted. The concentration fold change is calculated by dividing the Clover concentration of the treatment well by the concentration of the non-treated well. n = 4 biological replicates were performed for the 1st screen, and n = 3 biological replicates were performed for the 2nd screen. **E.** Immunoblot of Rb after UBR5 knockdown by siRNA. Cells were treated with siRNAs for 24 hours, and then treated with DMSO or Palbociclib (1μM) for 24 hours before harvest. The lower band in the Rb blot indicates the un/hypo-phosphorylated Rb (marked by red star). **F.** Microscopy analysis of HMEC cells expressing the Rb (886-928) KTR sensor, which reflects Cdk activity. Cells were treated with Ctrl siRNA or *UBR5* siRNAs for 48 hours. The cytoplasmic-to-nucleus intensity ratio of the KTR sensor is plotted against DNA content (DAPI staining). The dot color indicates the Rb concentration. **G.** Quantification of Rb concentration in different phospho-Rb populations shown in (F). Bars indicate mean and its 95% confidence interval. **H.** Degradation traces and the calculated half-lives of Clover-3xFlag-Rb after *UBR5* knock down. Box plot indicates 5th, 25th, median, 75th and 95th percentiles. **I.** Schematic of the *Fah-/-* mouse liver model and experimental flow. 6-week old *Fah-/-* mice were hydrodynamically transfected with plasmids carrying an *Fah-P2A-Cas9-sgNT* transposon or an *Fah-P2A-Cas9-sgUbr5* transposon, together with a transposase plasmid. 8 weeks later, hepatocytes were isolated from the mice for downstream analysis. **J.** Rb concentration in the low-phospho-Rb population of the primary hepatocytes isolated from mice receiving *Fah-P2A-Cas9-sgNT* or *Fah-P2A-Cas9-sgUbr5* transposons. The error bars indicate the standard deviation of the mean. **K.** Model schematic: Un-phosphorylated Rb is targeted for degradation by the E3 ligase UBR5 in early G1.

681 **Fig. 4**

682

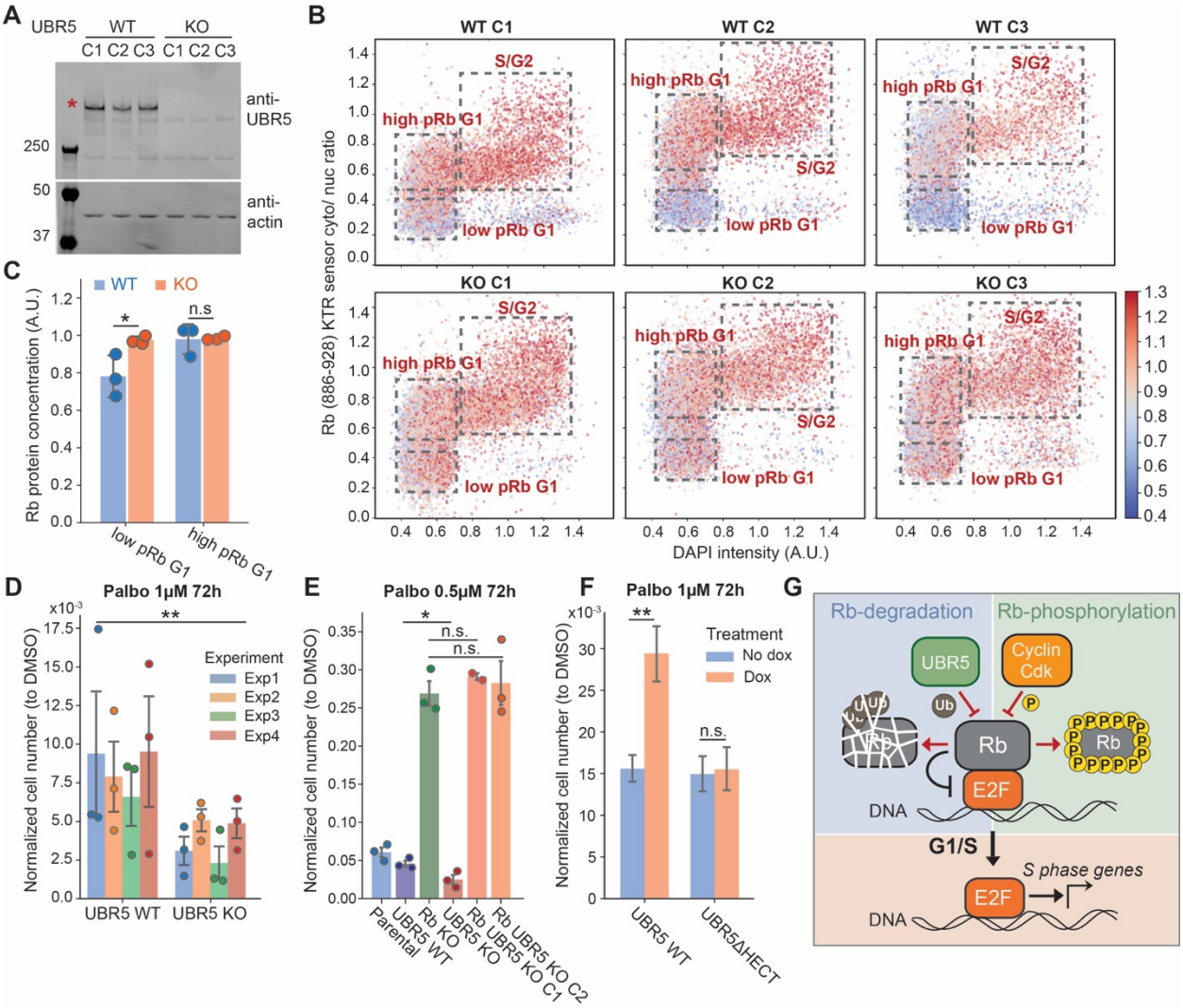

683

684

Fig. 4. UBR5 deletion sensitizes cells to CDK4/6 inhibition

A. Immunoblot verification of *UBR5 KO* clonal cell lines. **B.** Rb staining in *UBR5 WT* or *KO* clonal cell lines expressing the Rb (886-928) KTR sensor. The cytoplasmic-to-nucleus intensity ratio of the KTR sensor is plotted against DNA content (DAPI staining). The dot color indicates the Rb concentration. **C.** Quantification of Rb concentration in different phospho-Rb populations shown in (b). Circles denote results from individual clones and the bars denote the standard deviation. **D.** Normalized cell number of *UBR5 WT* or *KO* clonal cell lines after Palbociclib (1μM) treatment for 72 hours. Drug treatment started the day after plating. After 72 hours of drug treatment, cells were fixed and the cell number in each well was measured. Normalized cell number is the cell number under Palbociclib treatment divided by the cell number under DMSO control treatment. N = 4 biological replicates and error bars indicate the standard deviation. **E.** Normalized cell number of *UBR5 WT*, *RB1 KO*, or *RB1 UBR5* double *KO* clonal cell lines after Palbociclib (0.5μM) treatment for 72 hours. N = 3 biological replicates. **F.** Normalized cell number of UBR5 WT addback or UBR5ΔHECT addback cells after Palbociclib (1μM) treatment for 72 hours. GFP-UBR5 WT or GFP-UBR5ΔHECT were induced by Dox (100ng/ml). The results show the average from 3 *UBR5 KO* clonal cell lines with different UBR5 variants added back. We performed 3 biological replicates. The error bars indicate the standard deviation. **G.** Model schematic showing Rb is targeted for degradation by UBR5 in parallel to the canonical Rb phosphorylation pathway controlling Rb activity and thereby the G1/S transition.